Elkins-Tanton, L.T., et al., 2020, Field evidence for coal combustion links the 252 Ma Siberian Traps with global carbon disruption: Geology, v. 48, https://doi.org/10.1130/G47365.1

Field evidence for coal combustion links the 252 My-old Siberian Traps with global carbon disruption

Linda T. Elkins-Tanton, S.E. Grasby, B. Black, R.V. Veselovskiy, O.H. Ardakani, F. Goodarzi

SUPPLEMENTAL MATERIAL

Rock-Eval6 analysis

Dry samples weighing 70 mg were finely ground and analyzed using standard Rock-Eval 6 ® (Vinci Technologies, France) (Lafargue et al., 1998). The pyrolysis portion of the standard cycle used an iso-temperature of 300°C for 3 minutes followed by increasing temperature at a rate of 25°C per minute up to 650°C. The amount of hydrocarbon (mg HC/g Rock) released during the "pyrolysis stage" of Rock-Eval analysis is measured using the S1 and S2 peaks. Simultaneously, the amount of CO and CO_2 released during pyrolysis and then oxidation was measured to quantify the portion of oxygen-containing organic matter (S3 peak; mg CO_2/g Rock) and refractory residual carbon (RC), respectively. Total organic carbon (TOC) measured as sum of pyrolysable carbon (PC) and RC. Mineral carbon was obtained as the sum of the CO and CO_2 released during both pyrolysis and oxidation, at a higher temperature range. Total carbon (TC) measured as the sum of TOC and mineral carbon. Rock-Eval data were cross-checked using an internal standard reference material (Second White Specks Shale 9107) (Ardakani et al., 2016). Measured parameters have an accuracy and precision within 3% of the reference standard values.

Organic Petrology

Organic petrology was carried out on total 22 polished pellets from four sections of the Siberian flood basalt province to investigate the organic matter composition of the samples and random vitrinite reflectance (Ror) measurements (Table A1). The blocks made with a cold-setting epoxy–resin mixture. The resulting sample pellets were ground and polished, in final preparation for microscopy, using the LECO GPX200 grinding/polishing instrument. An incident light Zeiss Axioimager II microscope system equipped with a fluorescent light source and the Diskus-Fossil system was used for the petrology and reflectance measurements. Fluorescence microscopy of organic matter was carried out using ultraviolet G 365 nm excitation with a 420 nm barrier filter. Random reflectance measurements were conducted under oil immersion (objective ×50) following ASTM standard (ASTM, 2011). The standard reference used for reflectance measurements was yttrium-aluminum-garnet with a standard reflectance of 0.906% under oil immersion.

Definitions of Maceral Types 1, 2, and 3 thermal alterations of coal used in this paper

Maceral Type 1 include large individual coal fragments that predominantly consist of vitrinite with a mean random reflectance (Ror) of 0.56% (Fig A1a). Vitrinite macerals are scattered in the matrix of the volcaniclastic host rock. Those marginal sub-bituminous to high volatile bituminous coal fragments only show the effects of low thermal stress, including minor fracturing (Figs. 3a-c), along with some devolatilization features such as the development of desiccation cracks (Figs. 3a-f). Coal fragments also include liptinitic macerals, such as sporinite and cutinite, which show orange fluorescence under ultraviolet light (Fig. 3d), that further indicates these particles have only experienced low thermal stress. Other samples also contain more abundant and relatively higher rank (i.e. high-volatile bituminous) coal fragments consisting of vitrinite (Fig. 3e-f) with higher Ror value of 0.83% (Fig. A1b). Liptinitic macerals

mainly do not show fluorescence under ultraviolet light, indicating they have experienced higher thermal stress (Fig. 3e-f). This is indicative of heating of coal particles by close contact with hot volcaniclastic particles that resulted in increased thermal maturity of vitrinite macerals. Maceral Type 2 with Ror > ~2% have bright oxidation rims (Figs. 3g-h) due to exposure to elevated temperature. The bright rim indicates the exposure of those particles to higher temperatures, with partially burnt high-temperature char formed on the outer surface of less altered organic matter. The majority (~70%) of char particles are isotropic (Fig. 3g-l) which in some cases they still preserved the internal structure of woody matter (Fig. 3g-h). The outer rim of char particles shows Ror values up to 4%, along with minor contraction cracks. The majority of other isotropic char particles show a uniform texture without any internal structure (Fig. 3i-l). Maceral Type 3 is characterized by cenospheres and char particles formed from reactive organic fragments embedded in the volcaniclastic rock matrix (Fig. 3k-l). Two types of cenospheres, isotropic (~70%) and anisotropic (~30%) were observed in the studied samples. Cenospheres are found as a common by-product of modern coal combustion through injection of molten coal droplets into flu gas, causing rapid quenching(Goodarzi and Hower, 2008). Cenospheres thus result from rapid heating to high temperatures, followed by rapid cooling. They are rarely reported in the pre-industrial sedimentary record but have been observed in sediments at the Permo-Triassic boundary in the Sverdrup Basin of northern Canada (Grasby et al., 2011). Cenospheric particles in our Siberian Traps samples (Figs. 3k-n) display rounded devolatilization vacuoles and fine granular morphology and a semi-graphitic morphology with very high reflectance (Ror ~ 6%). Type 3 particles also include char, which is observed as rounded and angular fragments of combusted organic matter (Figs. 3k-n). Cenospheres have high Ror values ranging from 6 to 11% and in some cases developed anisotropy (Fig. 3m-n). The presence of

isotropic and anisotropic cenospheres suggest a combination of coal combustion/coking as well as significant forest fire due to volcanism. A wide range of type 3 macerals with high thermal alteration presented in Fig. A2.

FIGURES AND TABLES for SUPPLEMENTAL MATERIAL

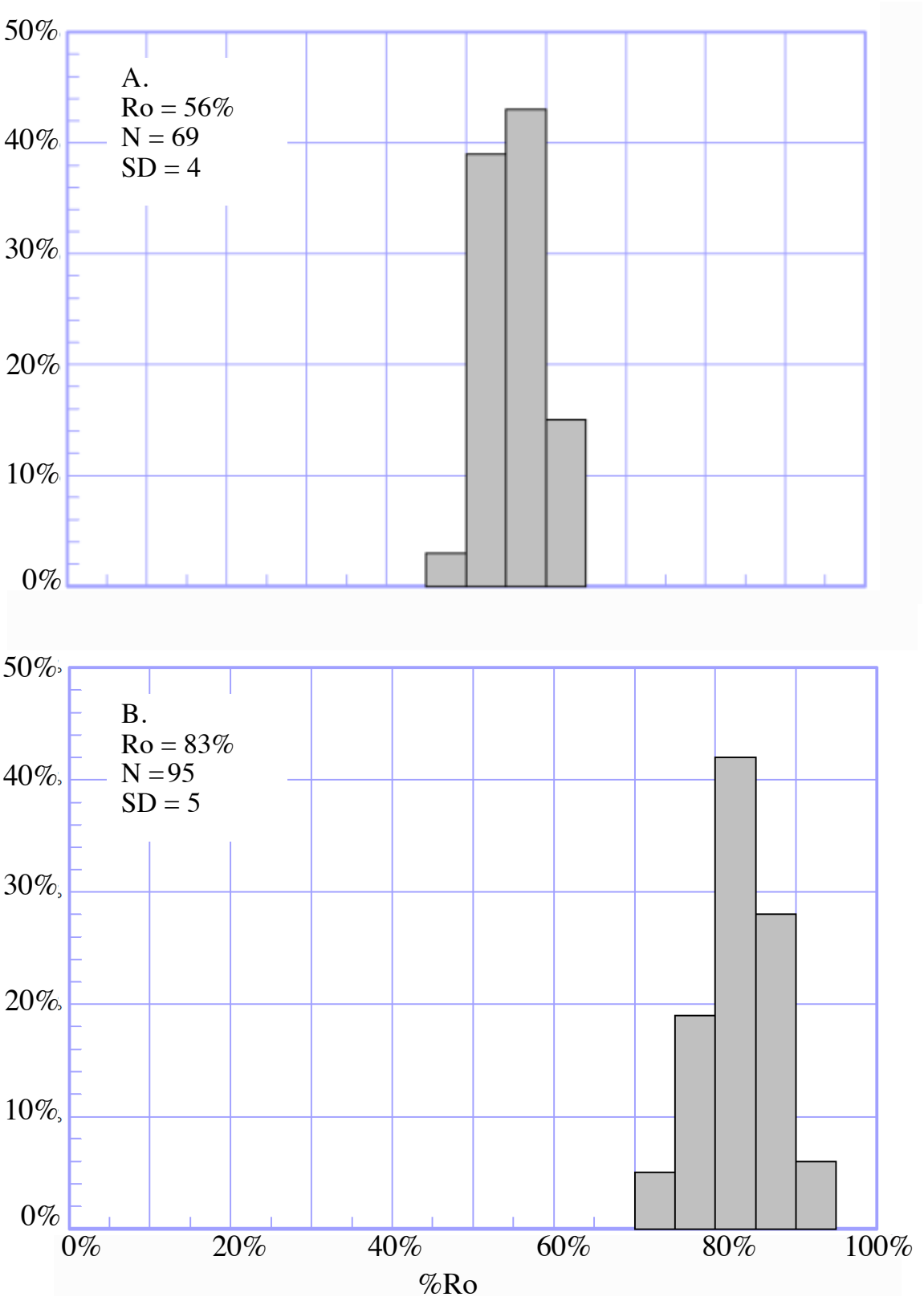

Fig. A1. Reflectograms (random reflectance) of low (A) and medium (B) thermally-altered coal particles.

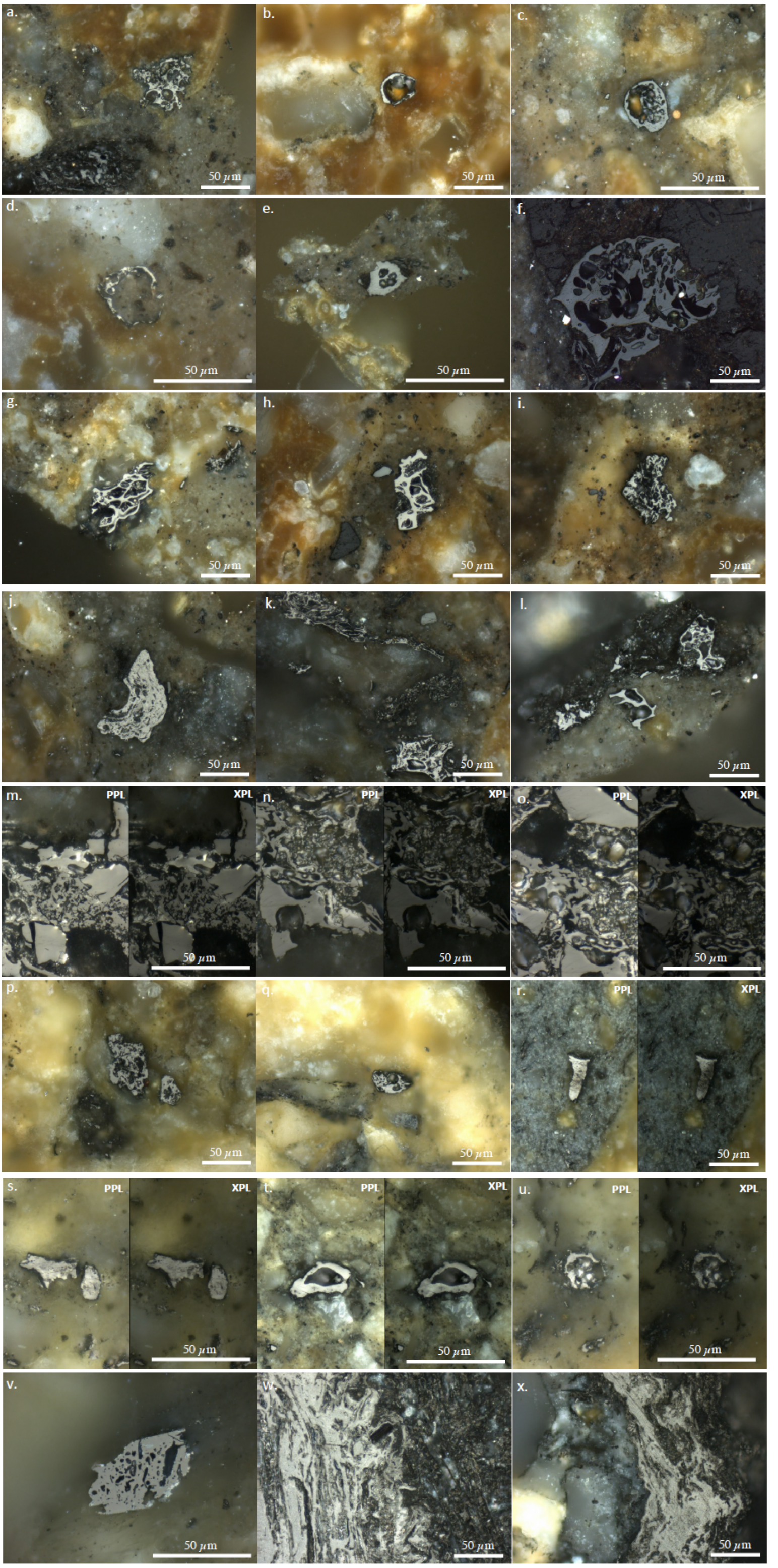

Figure A2. Photomicrographs of organic matter in the Siberian Traps. All photos are taken under reflected white light and oil immersion ×50 objective unless specified. a-f) Isotropic cenospheres in the matrix of volcaniclastic rocks, g-l) isotropic char particles in the matrix of volcaniclastic rocks, m-o) anisotropic cenospheres and char particles under plan polarized (PPL) and cross polarized (XPL) light, figures a-o are from location NT12-6.2. p-q) Isotropic cenospheres in the matrix of volcaniclastic rocks, r-u) anisotropic char and cenospheres in the matrix of volcaniclastic rocks under plan polarized (PPL) and cross polarized (XPL) light, figures p-u are from location NT12-15.1. v) Isotropic cenosphere from location R06-12A. w-x) Isotropic char particles resulted from combustion of woody particles from plants. The internal structure of organic matter is preserved in these samples, figures w-x are from location A10-7.1.

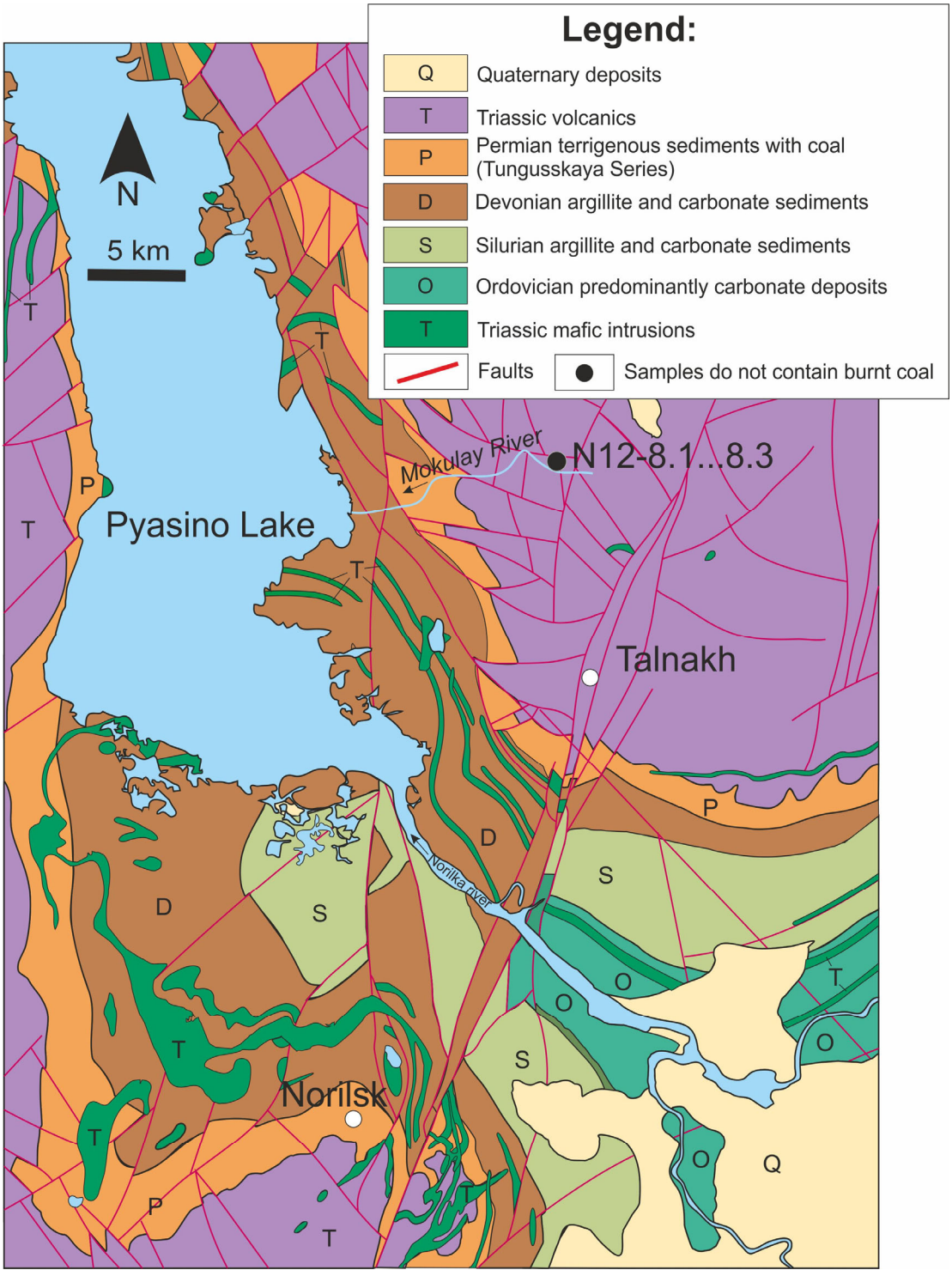

Figure A3.

Norilsk area: Detailed map showing samples analyzed for this study. Map after Malich et al. (1974).

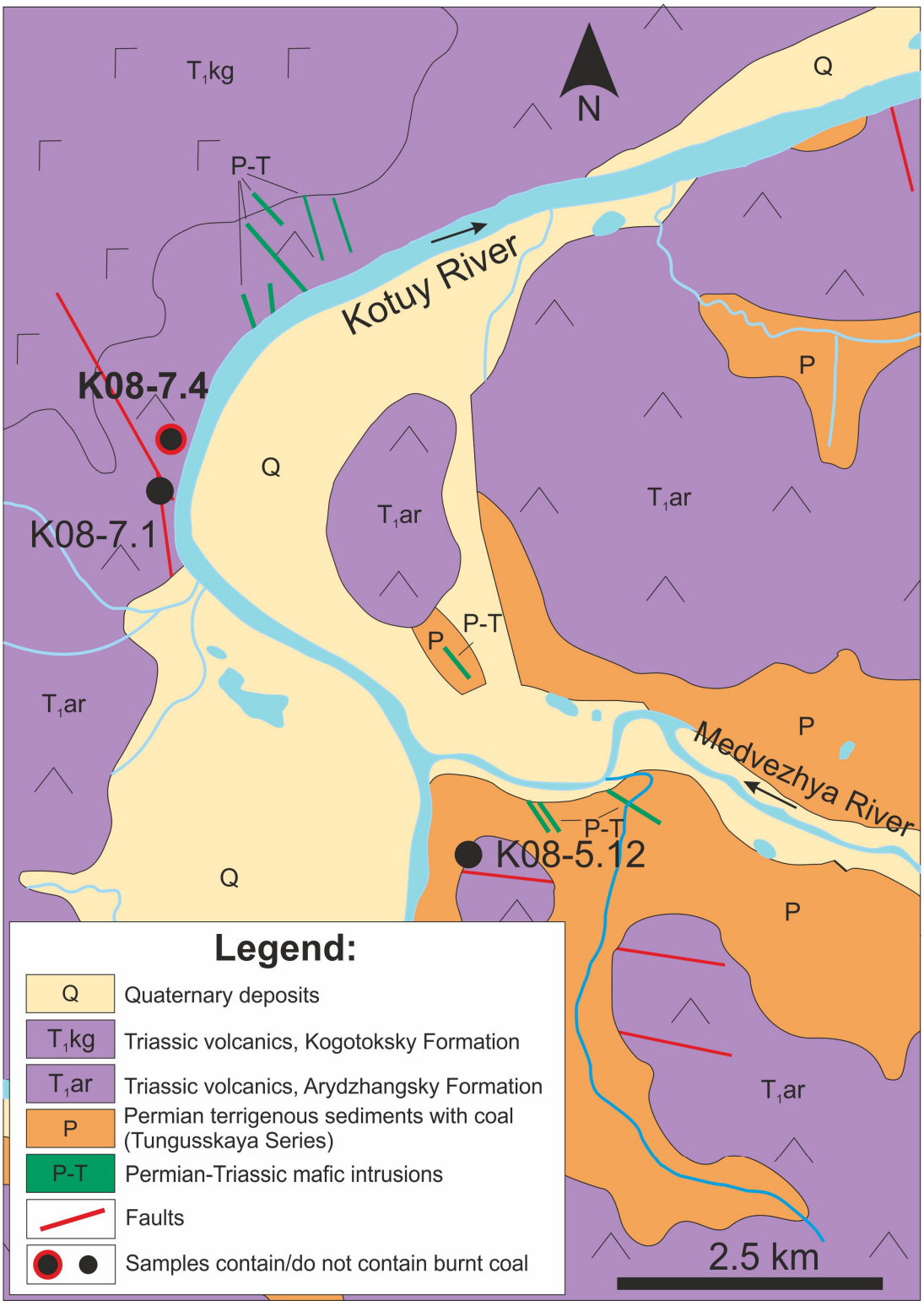

Figure A4.

Kotuy River area: Detailed map showing samples analyzed for this study. Map after after Malich et al. (1974).

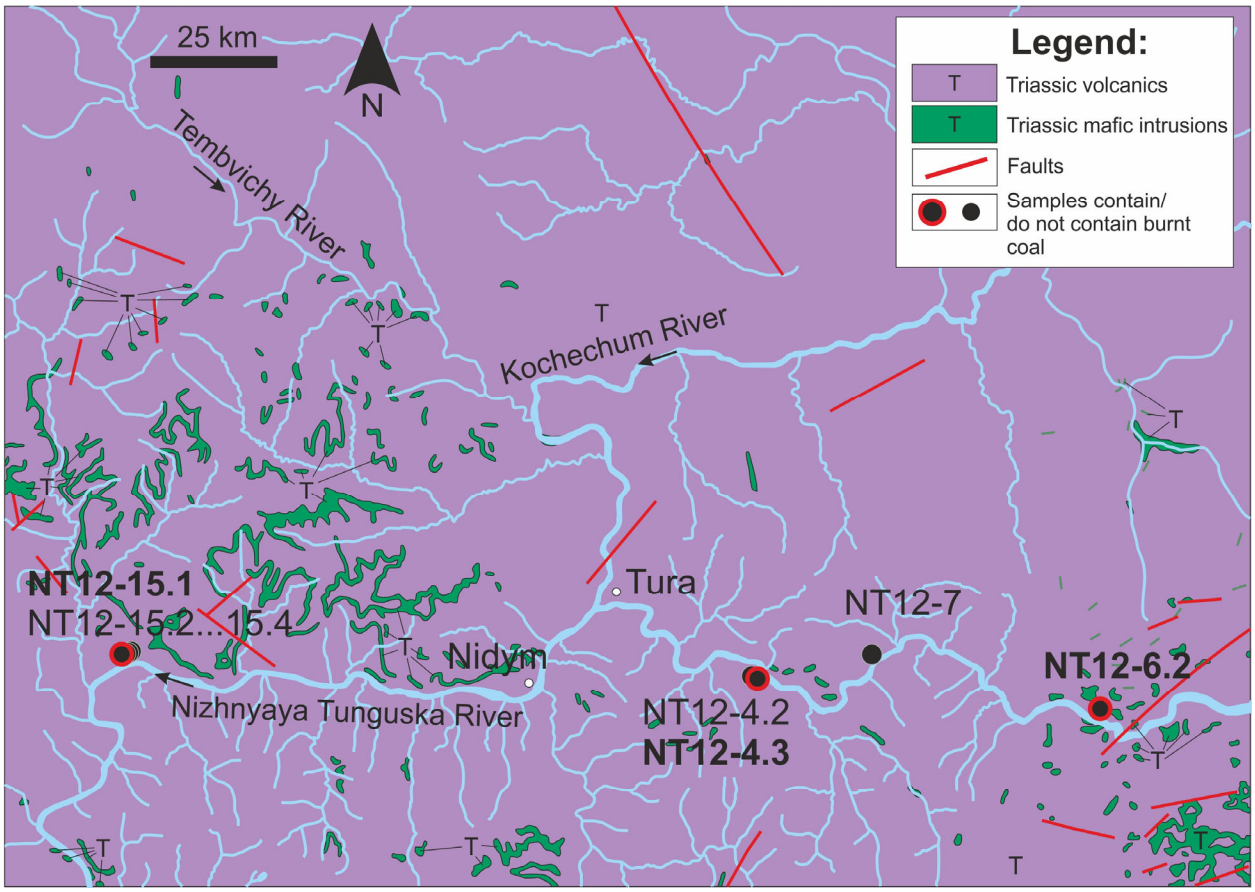

Figure A5.

Nizhnyaya Tunguska River area: Detailed map showing samples analyzed for this study. Map after Malich et al. (1974).

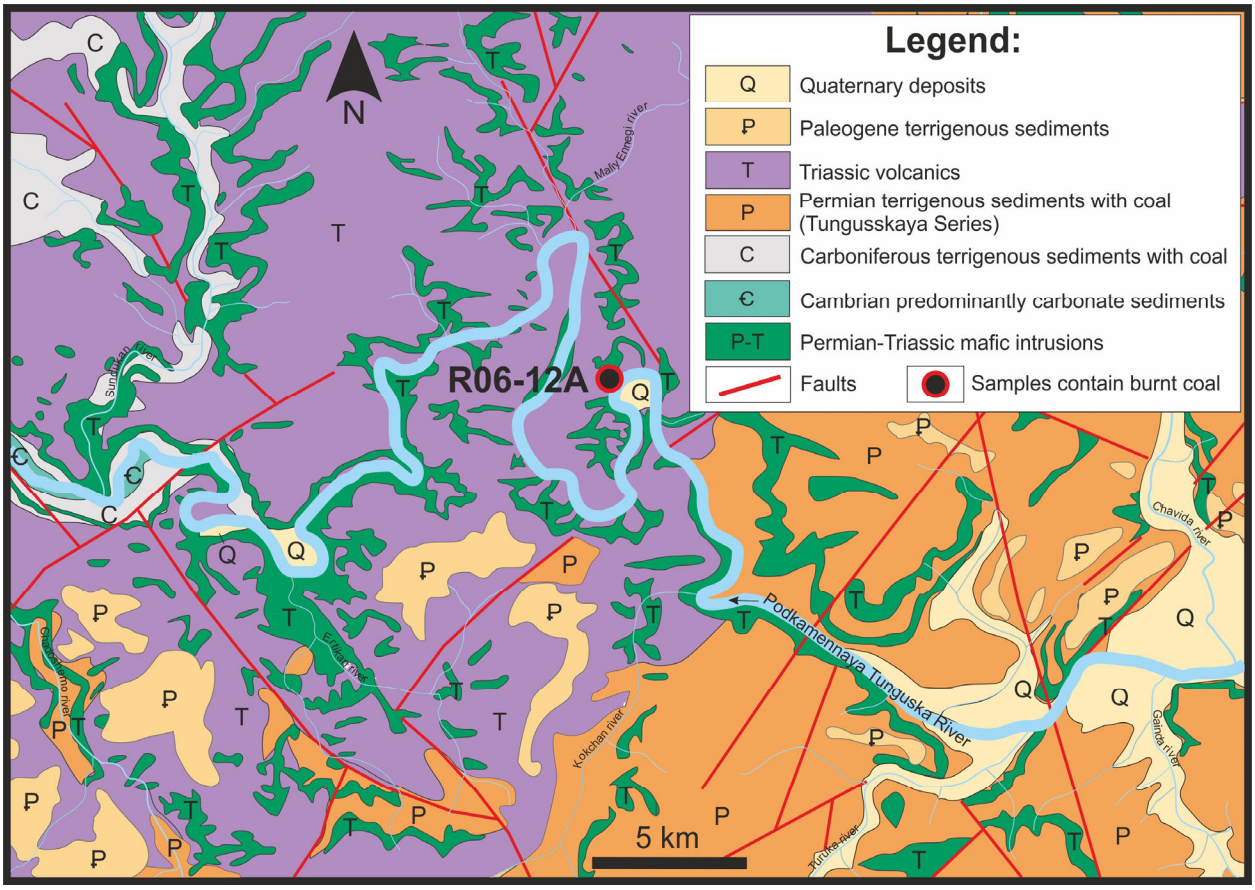

Figure A6.

Podkamennaya Tunguska River area: Detailed map showing samples analyzed for this study. Map after Malich et al. (1974).

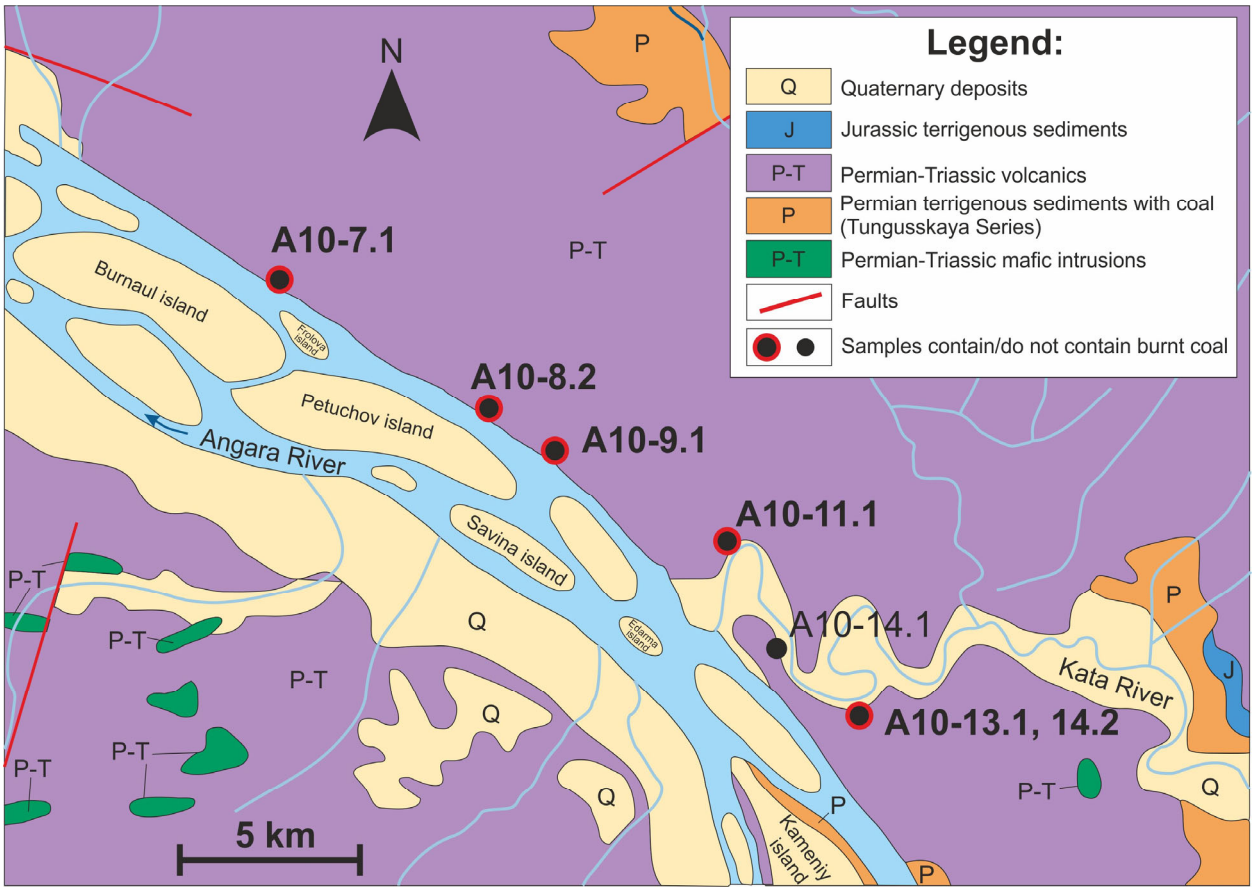

Figure A7.

Angara River area: Detailed map showing samples analyzed for this study. Map after Malich et al. (1974).

Table A1. Rock-Eval results of studied samples.

Sample[a]	C#[b]	TOC[c] wt. %
Nizhnyaya Tunguska River		
NT12-4.2	C-580294	1.16
NT12-4.3	C-580299	47.77
NT12-6.2	C-580293	0.39
NT12-7	C-580292	0.44
NT12-15.1	C-580287	0.11
NT12-15.2	C-597434	0.08
NT12-15.3	C-597435	0.01
NT12-15.4	C-580286	0.04
Norilsk Region		
N12-8.1	C-580291	0.38
N12-8.2	C-580298	0.35
N12-8.3	C-580290	0.35
Angara River		
A10-7.1	C-580297	0.30
A10-8.2	C-580284	0.02
A10-9.1	C-580285	0.57
A10-11.1	C-580283	0.27
A10-13.1	C-580282	0.01
A10-14.1	C-580289	0.62
A10-14.2	C-596833	0.36
Podkamennaya Tunguska River		
R06-12A	C-597436	0.21
Kotuy River		
K08-5.12	C-597437	0.02
K08-7.1	C-597438	0.06
K08-7.4	C-597439	0.06

Notes:

a: Sample number in the main collection, held by L.T. Elkins-Tanton at Arizona State University.

b: Analysis number in the lab of Stephen Grasby, Canadian Geological Survey.

c: Total organic carbon.

Table A2. Specific carbon contents of coal types (Keeling, 1973) used in calculations in the main text.

Dry Fuel	Kg C/Kg Fuel
Anthracite	0.90
Bituminous	0.72 – 0.82
Lignite	0.50
Peat	0.46
Wood	0.40

REFERENCES CITED IN SUPPLEMENTAL MATERIAL

Ardakani, O. H., Sanei, H., Snowdon, L. R., Outridge, P. M., Obermajer, M., Stewart, R., Vandenberg, R., and Boyce, K., 2016, The accepted values for the internal Geological Survey of Canada (GSC) 9107 Rock-Eval 6® standard (Upper Cretaceous Second White Speckled Shale, Colorado Group), western Canada.

ASTM, 2011, Standard Practice for Preparing Coal Samples for Microscopical Analysis by Reflected Light, Volume D2797/D2797M-11a: West Conshohocken, PA, ASTM International.

Goodarzi, F., and Hower, J. C., 2008, Classification of carbon in Canadian fly ashes and their implications in the capture of mercury: Fuel, v. 87, p. 1949-1957.

Grasby, S. E., Sanei, H., and Beauchamp, B., 2011, Catastrophic dispersion of coal fly ash into oceans during the latest Permian extinction: Nature Geoscience, v. 4, p. 104-107.

Keeling, C. D., 1973, Industrial production of carbon dioxide from fossil fuels and limestone: Tellus, v. 25, p. 174-198.

Lafargue, E., Espitalie, J., Marquis, F., and Pillot, D., 1998, Rock-Eval 6 applications in hydrocarbon exploration, production, and in soil contamination studies: Revue de l'Institut Francais du Petrole, v. 53, p. 421-437.

Malich, N. S., Tazihin, N. N., Tuganova, E. V., Bunzen, E. A., Kulikova, N. G., Safonova, X., Ivapoa, V. B., Baskov, E. A., P.O., G., Gavrikov, S. I., Golovanova, M. P., Gogina, N. I., Gorshkova, N. I., Grozdilov, A. L., Gromova, A. I., Egorov, L. S., Ivanova, A. M., Isaeva, L. L., Kljuchanskyi, N. G., Kolobova, N. I., Kutejnikov, E. S., Leonov, B. N., Ledneva, V. P., Mironjuk, E. P., Mihajlov, M. V., Mishnin, V. M., Stavtsev, A. L., Stulov, A. T., Shahotko, L. I., Schtein, L. F., Tsekhomskyi, A. M., and Yanova, E. N., 1974, Map of geological formations of the Siberian platform cover (1:1 500 000).